PAPER

Controlling the number of layers in graphene using the growth pressure

IOP Publishing Nanotechnology
Nanotechnology 30 (2019) 235602 (10pp) https://doi.org/10.1088/1361-6528/ab0847

Controlling the number of layers in graphene using the growth pressure

Joon Hyong Cho[1,4], Seung Ryul Na[2,4,5], Saungeun Park[3], Deji Akinwande[3], Kenneth M Liechti[2,5] and Michael A Cullinan[1,5]

[1] Department of Mechanical Engineering, The University of Texas at Austin, Austin, TX 78712, United States of America
[2] Department of Aerospace Engineering and Engineering Mechanics, The University of Texas at Austin, Austin, TX 78712, United States of America
[3] Department of Electrical and Computer Engineering, The University of Texas at Austin, Austin, TX 78712, United States of America

E-mail: seungryul.na@gmail.com, kml@mail.utexas.edu and michael.cullinan@austin.utexas.edu

Received 16 December 2018, revised 30 January 2019
Accepted for publication 19 February 2019
Published 25 March 2019

Abstract

Monolayer graphene is commonly grown on Cu substrates due to the self-limiting nature of graphene synthesis by chemical vapor deposition (CVD). Consequently, the growth of multilayer graphene by CVD has proven to be relatively difficult. This study demonstrates that the number of layers in graphene synthesized on a copper substrate can be precisely set by controlling the partial pressure of hydrogen gas used in the CVD process. This study also shows that a pressure threshold exists for a distinct transition from monolayer to multilayer graphene growth. This threshold is shown to be the boundary where the graphene growth process on Cu by CVD is no longer a self-limiting process. In addition, the multilayer graphene synthesized through the pressure control method forms in the Volmer–Weber mode with an AB stacking structure.

Supplementary material for this article is available online

Keywords: multilayer graphene, chemical vapor deposition, graphene electronics

1. Introduction

Bilayer and multilayer graphene have found many uses in a range of applications from low resistance flexible transparent electrodes [1] to corrosion protection [2, 3] to roll-to-roll electronics manufacturing [4–6]. For example, bilayer graphene has a tunable bandgap [7] and is ideal for tunnel field effect transistors [8, 9]. However, the precise fabrication of bilayer or multilayer graphene with a controlled number of layers is extremely difficult. Most attempts to produce bilayer or multilayer electronic devices have relied on the attempting to find sections of bilayer/multilayer graphene on samples exfoliated from bulk graphite samples [10–13]. The results from these devices are encouraging with a band-gap up to 0.25 eV demonstrated for bi-layer graphene produced by this mechanical exfoliation method [7]. However, this method is not scalable to the large-scale production needed for electronics manufacturing. Therefore, various studies attempted to produce bi- or multi-layer graphene with an AB lamination structure using chemical vapor deposition (CVD), which is a more scalable graphene fabrication method.

Unfortunately, the controlled fabrication of bilayer or multilayer graphene by CVD has proven to be difficult. Most CVD graphene is grown on copper substrates because of the self-limiting nature of graphene growth on copper [14]. In CVD graphene grown on copper, the copper surface that serves as the catalyst for graphene synthesis becomes covered with the graphene which prevents the copper from catalyzing more graphene growth and thus inhibiting multilayer graphene growth [15]. One approach to overcome this challenge has been to grow graphene on Cu–Ni alloys [16, 17]. The presence of Ni in the Cu–Ni alloy helps to increase the carbon solubility in the alloy and thus promotes multilayer growth.

[4] These authors contributed equally to this work.
[5] Authors to whom any correspondence should be addressed.

However, the increased carbon solubility makes growing uniform graphene on these Cu–Ni alloys difficult, which generally results in large variances in the number of layers across the sample grown using this method [17, 18].

Recent research has reported that it is possible to synthesize multi-layer graphene by either changing the carbon to hydrogen ratio or increasing the partial pressure of hydrogen during the CVD growth process [19, 20]. Liu [21] has reported the successful synthesis of multilayer graphene by controlling the hydrogen partial pressure while supplying hydrogen and methane. Luo also reported that multilayer graphene can be synthesized through dynamic control of pressure in the process of graphene synthesis [22]. However, the ability to precisely control the growth of bilayer or few-layer graphene with a set number of layers has yet to be demonstrated or analyzed. Therefore, the purpose of this study is to quantify the effect that the hydrogen partial pressure has on the growth of bilayer and multilayer graphene in order to understand the role of pressure in multilayer graphene growth and to be able to precisely grow bilayer or few-layer graphene.

2. Experimental section

This section outlines how the graphene was grown on copper foil and how it was transferred to the SiO_2 surface of a silicon chip for characterization.

2.1. Graphene growth on copper foils

In this work, the graphene growth was performed with on copper foils (thickness of 130 μm and purity of 99.95%, Alfa Aesar) as the metal catalyst. The Cu foil was 1 × 6 inches and was chemically treated in a 0.1 M ammonium persulfate solution (APS) for 30 min to remove the layer of native copper oxide as well as other contaminations that exist on the copper foil. This was followed by sequentially cleaning the copper in acetone, isopropyl alcohol (IPA), and de-ionized (DI) water bath. The treated copper foil was placed in the middle of a quartz tube in the growth furnace. Graphene growth was then preformed according to the following steps: (1) the pressure in the quartz tube was pumped down to 10 mTorr, (2) the copper foil was heated to 1030 °C under a flow of hydrogen gas of 10 standard cubic centimeters per minute (SCCM) in the quartz tube; (3) the specific pressure for graphene-growth was set by controlling the down flow valve of the CVD system under a constant temperature (1030 °C) and hydrogen environment (pressures of 0.47, 10, 40, 50, 80, and 120 Torr were selected for the multilayer graphene growth); (4) graphene growth was then conducted with two mixtures of hydrogen and methane at 10 SCCM and 0.1 SCCM for 30 min at 1030 °C, respectively; (4) the entire CVD system was naturally cooled while flowing the gas mixtures and the coated copper foil was removed for analysis. (For details, see figure S1 in supplementary information, available online at stacks.iop.org/NANO/30/235602/mmedia.)

2.2. Transfer of graphene to silicon oxide substrates and electrical measurements

In order to evaluate the properties of graphene, as-grown graphene on the copper foil was transferred to 300 nm thick silicon oxide substrates on silicon, SiO_2/Si (100), by the typical poly(methyl methacrylate) (PMMA) assisted wet transfer technique. The PMMA (100 K molecular weight, Microchem) was spin-coated on the graphene on the copper foil at the rate of 4000 RPM for 45 s. After pre-curing the PMMA/graphene/Cu foil/graphene composite at 190 °C for 20 min, the graphene without PMMA beneath copper foil was etched by exposing it to an O_2 plasma environment [23] for 10 s. The sample was then placed in an APS solution of 0.1 M for 10 h to etch away the copper foil and leave behind PMMA/graphene floating on top of the APS solution. The thin PMMA/graphene film was cleaned in DI water and then transferred onto SiO_2/Si substrates and stored in a vacuum desiccator to remove trapped water between PMMA/graphene and the substrate. After drying the sample overnight, stronger adhesion between graphene and the substrate was achieved by baking the sample at 120 °C for 15 min. Finally, graphene-coated silicon was obtained by removal of the PMMA layer in an acetone bath for 60 min, followed by annealing under ambient conditions at 450 °C for 30 min in order to remove any of the remaining polymer residue on the sample [24]. For the electrical measurements of the graphene, Au/Cr electrodes with 4 different gap sizes of 25, 50, 100, and 200 μm were deposited on top of the graphene.

3. Results and discussion

Monolayer, bilayer and multilayer of graphene (three or more layers) were synthesized on the copper foil by the CVD process described above. Figure 1 shows a series of scanning electron microscope (SEM) images of as-grown graphene on copper foil at 0.47, 10, 40, 50, 80 and 120 Torr (see figures 1(a)–(f)), respectively (For larger scale SEM images, see figure S3 in supplementary information.)

As can be seen in figure 1, graphene grown at a pressure of 0.47 Torr (figure 1(a)) is a wrinkle free monolayer graphene whereas wrinkles are present under the higher-pressure growth conditions, indicating the presence of multilayer graphene. Only copper steps are visible on the graphene on Cu foil in figure 1(a). Though the origin of wrinkles in multilayer graphene is not well known [25, 26], it is hypothesized that the wrinkles (ML wrinkle in figures 1(b)–(f) represented as white lines in SEM) in the multilayer graphene most likely result from the formation of vacancies between layers in the graphene. As a result of the difference of the emissivity resulting from the vacancies between interlayers, these wrinkles appear as the bright lines in the SEM images [25, 27, 28]. These ML graphene wrinkles are distinguishable from monolayer graphene wrinkles because monolayer graphene wrinkles are darker in contrast. In addition, it can be observed in figure 1 that as the growth pressure increases, the overall contrast on the graphene in the images becomes darker

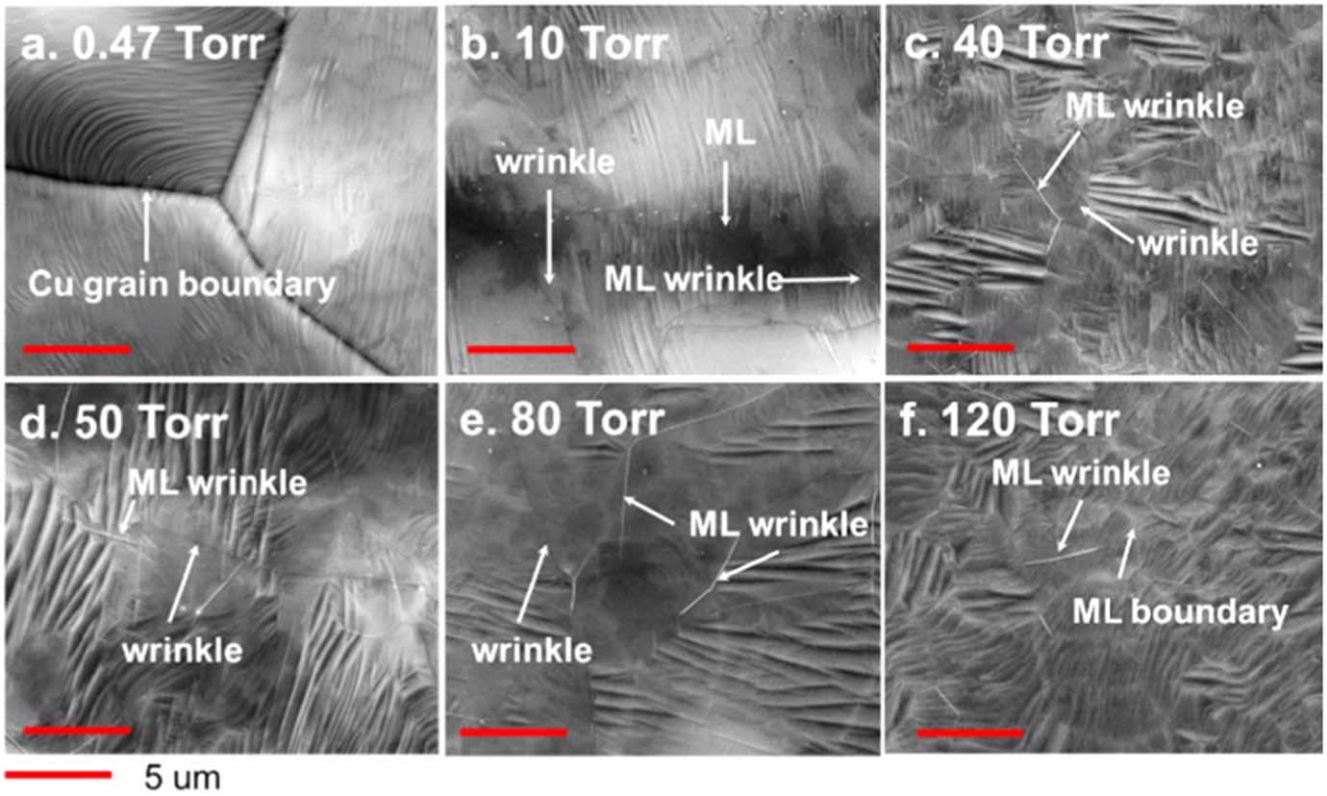

Figure 1. SEM of graphene grown on the copper foil at: (a) 0.47, (b) 10, (c) 40, (d) 50, (e) 80, and (f) 120 Torr where ML is an abbreviation for multilayer. The scale bar (red line at the bottom right corner) indicates 5 μm.

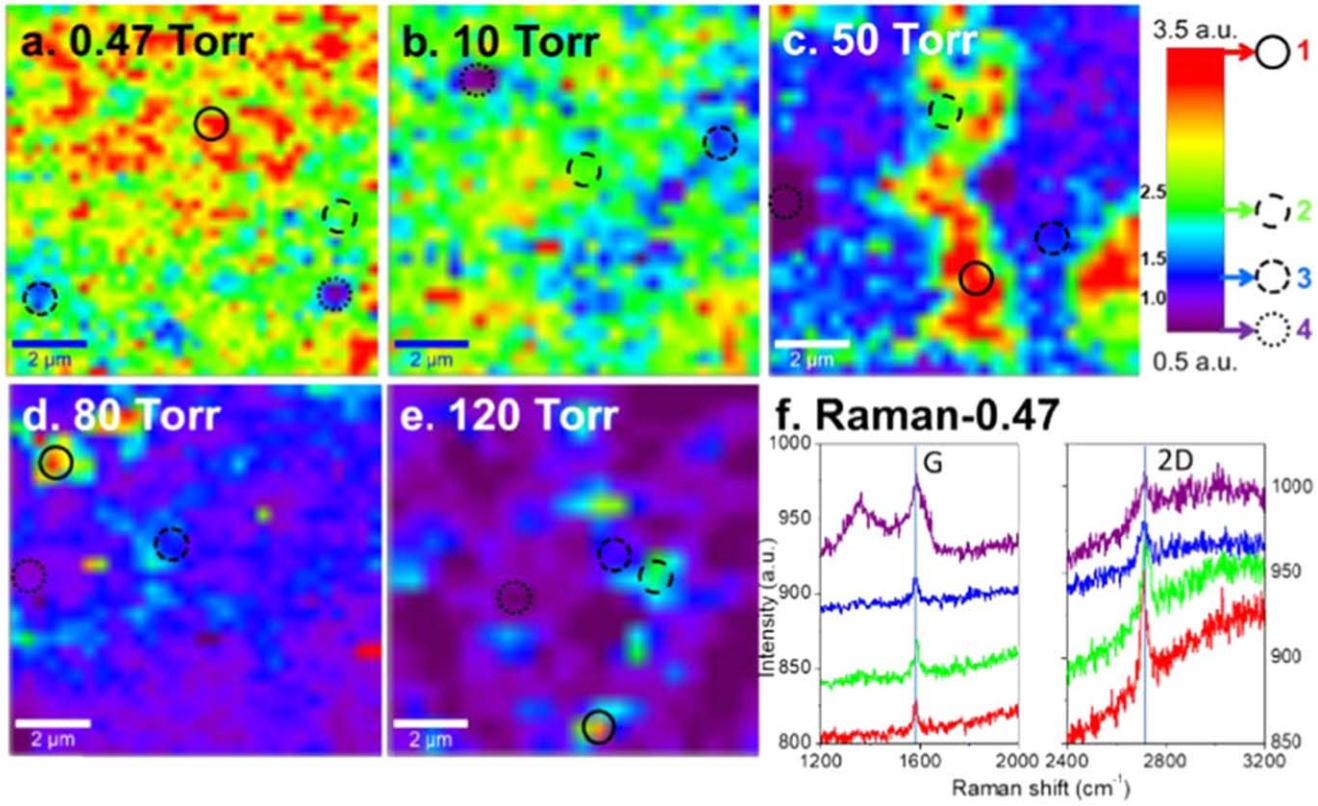

Figure 2. Raman responses of graphene on copper foil: Raman mapping of I_{2D}/I_G of (a) 0.47, (b) 10, (c) 50, (d) 80, (e) 120 Torr, and (f) Raman spectra of four selected regions of graphene at 0.47 Torr. The Raman mappings were conducted on an area of 10 $\times$ 10 μm. The Raman spectra of other cases (10–120 Torr) are given in the supplementary information figure S4.

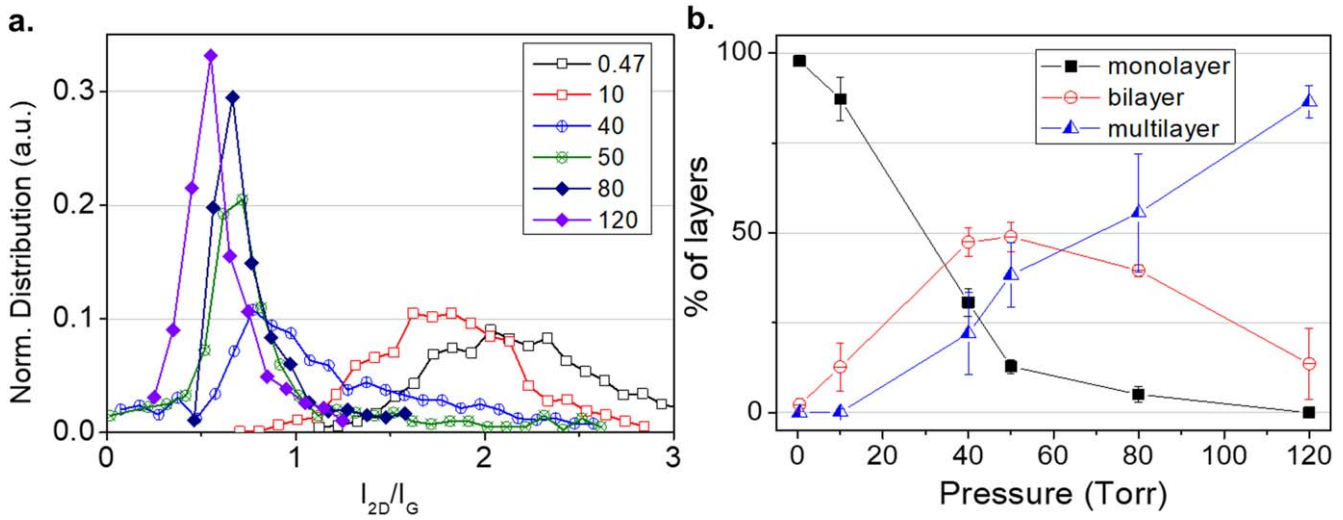

Figure 3. (a) Raman response of graphene as normalized distributions of I_{2D}/I_G. (b) The percentage of the number of layers as a function of growth pressure of which graphene was grown. The average percentage of the number of layers and associated error bars were analyzed from Raman intensity data in figure 3(a) by accumulating the area under the curve.

which further indicates that the number of graphene layers is increasing [29, 30].

To characterize the quality and number of layers of as-grown graphene on the copper foil, Raman spectroscopy (WITec Alpha 300 micro-Raman confocal microscope, $\lambda = 488$ nm) was conducted on the copper foil after graphene growth. Figures 2(a)–(e) are the images of the Raman mapping associated with the intensity ratio (I_{2D}/I_G) of G and 2D peak at growth pressures of 0.47, 10, 50, 80, and 120 Torr, respectively. In these Raman images, blue regions indicate the presence of bi-layer graphene and purple regions indicate multilayer graphene while the red and yellow-colored regions are monolayer graphene.

The Raman spectrum mapping image (see figure 2(a)) at 0.47 Torr shows that the entire surface was covered with monolayer graphene as evidenced by the fact that the intensity ratio between the 2D and the G peaks of Raman spectra (I_{2D}/I_G) is greater than two over the majority of the surface [17]. For the 10 Torr growth (figure 2(b)) shows that monolayer graphene is still dominant over the entire surface but that small spots of bi-layer graphene (see supplementary information in figure S4(a)) for the details of selected regions) are observable. In graphene growth with a pressure exceeding 10 Torr, the percentage of monolayer graphene starts to drop rapidly as increasing areas of bilayer and multilayer graphene are formed. At 50 Torr (see figure 2(c)), only about 20% of the scanned area of the mapping was covered with monolayer graphene and the rest of the area was bi-layer ($I_{2D}/I_G \sim 1$) and multilayer ($I_{2D}/I_G < 1$) as represented by the blue and purple domains, respectively. Further details of Raman spectra in the blue and purple regions are analyzed in figure S4(b). For the 80 Torr (see figure 2(d)) and 120 Torr (see figure 2(e)) cases, bi-layer or multilayer graphene covers most of the surface. (For the details of 80 and 120 Torr at the selected regions please see figures S4(c), (d) in supplementary information, respectively.) These Raman spectra results support the conclusion based on the contrast and presence of the wrinkles in SEM (see figure 1) that the number of graphene layers increases as the growth pressure increases.

Quantifying the effect of the growth pressure on the number of layers is important, therefore, we analyzed probability distribution functions of the I_{2D}/I_G intensity ratios calculated by examining each of the large area Raman scans for the different pressure growths on a pixel-by-pixel level as shown in figure 3(a). In general, as the pressure increases, the probability distribution function becomes broader indicating a wider range in the number of graphene layers present in the samples. These probability distributions were then used to calculate the percentage of monolayer, bilayer, and multilayer graphene in the growths as a function of the growth pressure as shown in figure 3(b). In this figure, the average of percentage of number of layers was determined by calculating accumulation of area under the curve where the area under the curve of I_{2D}/I_G range from 1.5 to 3.0 is considered monolayer, the range from 0.8 to 1.5 is considered bilayer, and below 0.8 is considered multilayer graphene. The error bars in figure 3(b) were calculated as the standard deviation of the layer number percentages between different Raman scans for growths with the given growth pressure.

As can be seen in figure 3(b), the percentage of monolayer graphene decreases as growth pressure is increased and the percentage of multilayer increases. The percentage of bilayer graphene is highest at the growth pressure of 50 Torr and more multilayer graphene starts being produced at higher pressures. This graph clearly shows that the amount of multilayer graphene rises with increasing growth pressure.

Raman spectroscopy is a convenient tool for determining number of graphene layers on Cu foil or on SiO_2/Si substrate; however, the Raman responses on multilayer graphene become ambiguous when the number of graphene layers is greater than three. For example, when the Raman response of I_{2D}/I_G ratio on graphene is below 0.75 (as is the case with growth pressures above 80 Torr), it is difficult to accurately evaluate the number of graphene layers since the more

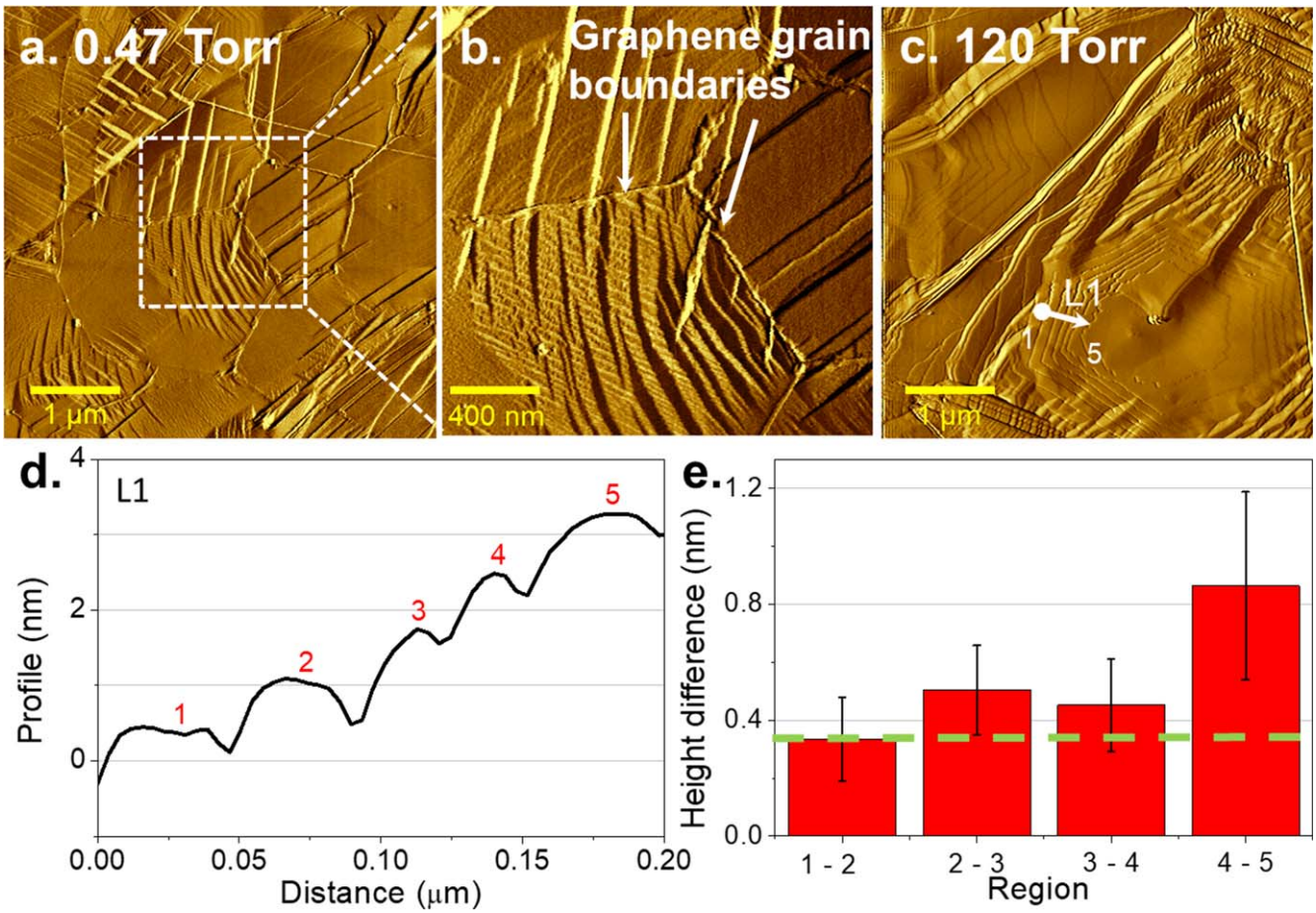

Figure 4. AFM image of graphene grown on copper foil: (a) graphene at 0.47 Torr, (b) high resolution image near copper oxide and graphene grains, (c) graphene at 120 Torr, (d) height profile of the graphene steps along the line L1, and (e) the height difference between each region.

graphene layers do not significantly affect the I_{2D}/I_G ratio. Thus, for precise measurement of the number of layers in the multilayer graphene grown in this study, atomic force microscopy (AFM, Park Scientific XE-100) was used. While obtaining morphology data from AFM, we also measured the lateral force spectrum of the surface, which helped us to visualize copper morphology as well as graphene steps.

The AFM image in figure 4(a) shows the morphology of a typical monolayer graphene/Cu foil surface grown at a pressure of 0.47 Torr over a $5 \times 5\,\mu$m area. The scanned regions are characterized by the hexagonal graphene domains (average radius is approximately 0.6 μm, see figures S8, 9 in supplementary information). The size of Cu grains in these foils were determined to be larger than 10 μm by SEM by observation in figure 1, therefore the hexagonal patterns in the AFM images are graphene grains [31]. In order to make sure that the hexagonal patterns are indeed graphene grain boundaries, a closer-up scan (see figure 4(b)) of the white rectangle in figure 4(a) is shown in which the details of copper steps in the hexagonal pattern are observable. The hexagonal patterns are also observed to be surrounded by ragged lines which are copper oxide formed at the defects at the interfaces of the of as-grown graphene grains.

AFM scans (see figure 4(c)) of graphene synthesized on copper foil at 120 Torr show that the hexagonal pattern grew radially and repeated for the multilayer graphene samples. If graphene layers are formed, the thickness difference at each step should be approximately 0.335 nm [32]. Figure 4(d) shows a line profile of height indicated in figure 4(c) as Line profile 1 on Copper (L1). Each step represents a graphene step counting from graphene '1' to graphene '5'. Each step height difference from the measurement is calculated by subtracting a morphology of copper surface from original AFM data as shown in figure 4(e) where average height difference from step to step is approximately 0.4 nm. Region 4–5 has height difference of 2 layers of graphene stacked which is calculated as 0.8 nm. Therefore, figure 4(e) suggests that approximately six layers of graphene were formed at the selected location on graphene.

In order to understand how the multilayer graphene grains grow and coalesce, graphene was produced by shortening the growth time. Total absorption time of 10 min instead of the original recipe of 30 min was used. Graphene grown on Cu foil in this manner under 120 Torr is shown in figures 5(a), (b) where a few graphene grains are produced before fully covering the surface of Cu foil.

Figure 5(a) exhibits a patch of multi-layer graphene, contacting with an adjacent region of multi-layer graphene. In addition, we can observe multilayer wrinkles (ML wrinkle) at the center of each graphene domain as well as where they

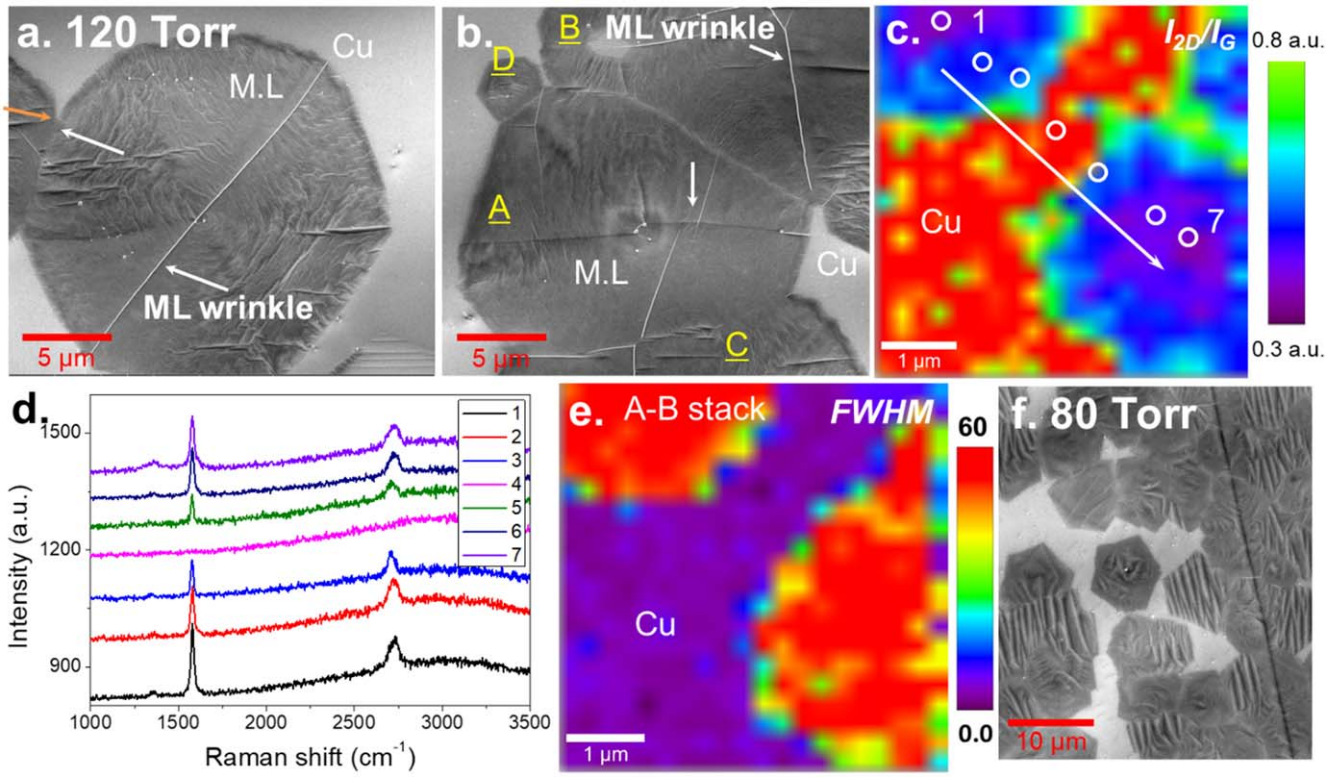

Figure 5. A demonstration of graphene growth: (a) SEM image of growth at 120 Torr, (b) SEM image at different locations, (c) Raman mapping (I_{2D}/I_G) of partially grown graphene on copper foil, (d) Raman spectra from point 1 to point 7, (e) the plot of FWHM, and (f) SEM image of partially grown graphene at 80 Torr.

merge. This is clear in figure 5(b), with the formation of a boundary (a white arrow) of multi-layer graphene grains (A–D) with several wrinkles in each domain. Figure 5(c) shows that the I_{2D}/I_G ratio of two nearby graphene patches varies from 0.3 to 0.8. This mapping image shows that when the graphene was formed on copper, the monolayer and bilayer graphene grew outward from the nucleation point and simultaneously formed more layers of graphene at the nucleation point. The white circles (see figure 5(c)) represent the locations (1–7) where the Raman spectra were observed on the sample. In figure 5(c), location 1 is the center of multilayer graphene which corresponds to the Raman spectrum labeled '1' in figure 5(d) with an I_{2D}/I_G ratio of 0.7. Due to the decrease of the ratio (I_{2D}/I_G) from point 2 to point 3, we estimated that tri and bi-layer graphene were formed at these points, respectively. The absence of the two characteristic peaks of graphene (point 4) supports the absence of the graphene layer on copper there. Along the points 5, 6, and 7, the Raman spectra indicate that bi-layer, tri-layer and few layers of graphene were formed, respectively. The FWHM of I_{2D} of graphene shown in figure 5(e) indicates that the majority of FWHM is close to 60, indicating AB stacking of graphene layers [33]. Thus, it is possible to conclude that the multilayer graphene grown on the copper was AB stacked graphene in each domain. When the growth process described above was repeated at 80 Torr, similar graphene growth patterns were observed (see figure 5(f)). These results indicate that the growth of the multi-layer graphene proceeds from the nucleation sites until the graphene patches merge together.

To accurately quantify the number of graphene layers that form in the multilayer domains, the multilayer graphene was transferred onto a silicon oxide surface and atomic force microscopy was used to measure the number of layers across multiple locations on the sample. The SEM image in figure 6(a) shows graphene grown at 120 Torr consisting of multilayers having visibly different contrast due to different numbers of layers of graphene at different regions in the sample. Multilayer graphene is also confirmed by the AFM mapping data in figure 6(b), where the hexagonal domains are defined by steps, multi-layer graphene wrinkles, and grain boundaries. When the height profile along L2 (see figure 6(c)) was measured along with the friction at each step using lateral force microscopy (LFM), it suggests that multilayer graphene growth is most likely to be stacked in the form of Volmer–Weber (VW) type graphene structures, in which additive layers are formed beneath monolayer graphene [20, 34], since there was no change in the measured friction at each step. The results are consistent with the expected growth mechanism given the low methane concentration ratio growth conditions used and the stacking sequence visible in figures 6(a), (b). In addition, the height variation at each step (see figure 6(d)) suggests that average graphene step heights of 0.38 nm are distinguishable within $\pm 0.1\ \mu$m. Height measurements of various wrinkles and boundary layers of graphene grains are presented in figures S8(a), (b) in supplementary information. The Raman spectra of the transferred graphene is shown in figure 6(e) where the ratio of peak intensities I_{2D}/I_G is mapped for the sample. The mapping shows that the majority

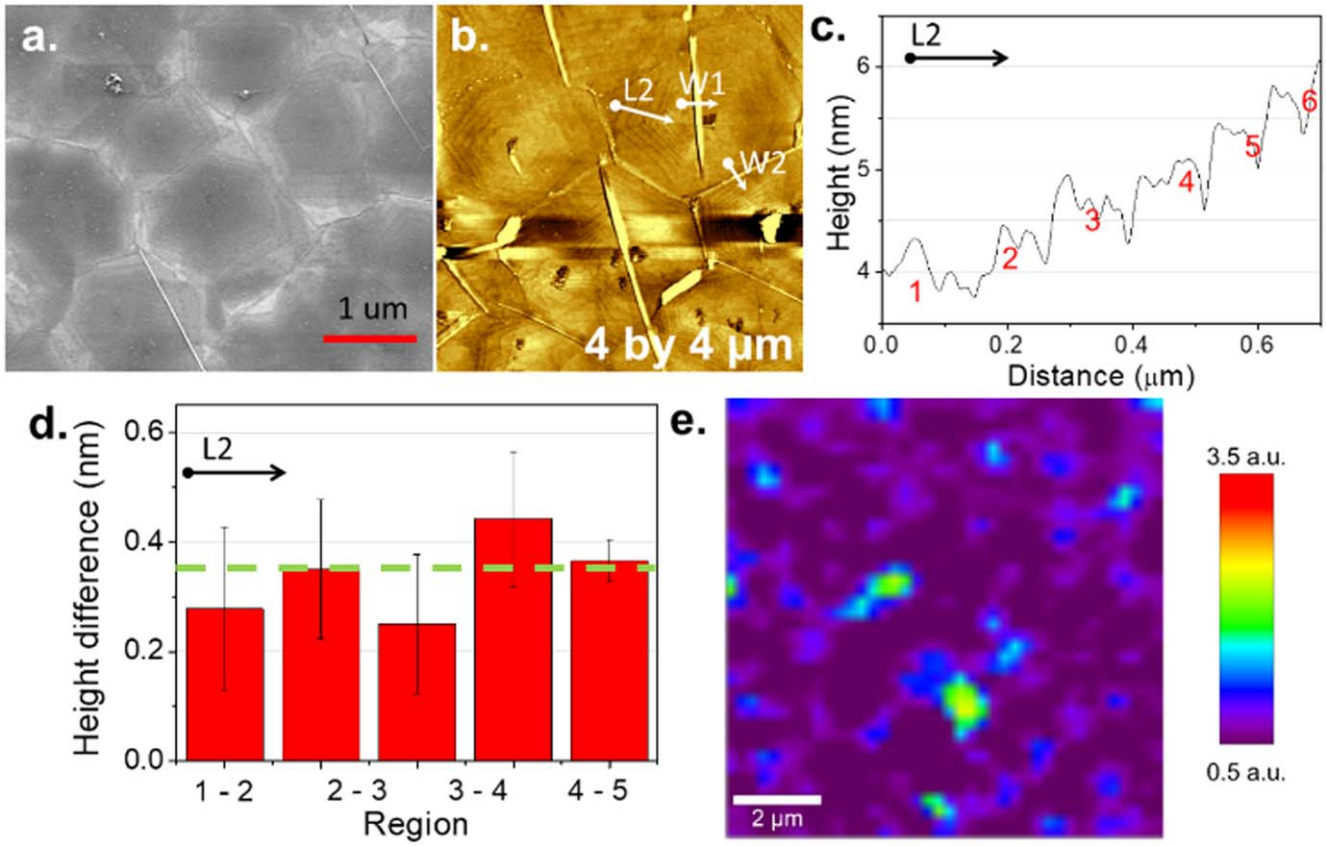

Figure 6. Diagnostics of the wet-transferred graphene on silicon oxide: (a) SEM image of the transferred graphene, (b) AFM image, (c) profile of graphene steps along line (L2), (d) height difference of graphene steps, and (e) Raman mapping (I_{2D}/I_G) of the graphene on an area of 10 × 10 μm.

of 10 × 10 μm area is covered with multilayer graphene ($I_{2D}/I_G \approx 0.5$) and that the boundaries of the graphene patches are close to bilayer graphene ($I_{2D}/I_G \approx 1$).

Statistical values gathered from both the Raman data in figure 3(a) and the AFM data (by counting the actual number of graphene layers in the transferred multilayer samples) were used to estimate the average number of layers and the possible range in the number of layers at each growth pressure.

Figure 7(a) shows number of graphene layers measured at the center of graphene grains as a function of the growth pressure in box chart where the top quarter and the bottom quarter of percentiles are represented by the rectangular boxes. The average value of each growth is marked as a line in the boxes. As can be seen in figure 7(a), the average number of graphene layers increases as the growth pressure increases and that the range in the number of layers found also increases as the pressure increases.

For growth pressures below 10 Torr, most of the graphene grown is monolayer but above 10 Torr the growth conditions start to exhibit an increased variation in the number of layers grown. A growth pressure of approximately 40 Torr appears to be the point where bilayer graphene starts to become the dominant graphene configuration. At 50 Torr, more multilayer graphene starts to grow so that while the average number of graphene layers remains at 2–3 layers. Overall, it is observed that, as as the pressure increases, there are small sections of the sample that contain far more than the average number of layers for that growth pressure. For example, when grown at 80 Torr, there can be up to 7 graphene layers while the average number of layers is only 4–5 and at 120 Torr, up to 11 layers were observed sporadically whereas the average number of layers is only 8. These spots of high layer counts show that new layers can quickly form at nucleation sites for the high-pressure growths when the graphene growth is no longer self-limiting.

It has been well-reported that the graphene growth at lower pressures is a self-limiting process, leading the formation of monolayer graphene on copper foil [15]. However, controlling the partial pressure of hydrogen prior to supplying methane shows that the self-limiting process can overcome, thereby enabling multilayer graphene growth on the surface of Cu foil. This study shows that growth pressures from 10 to 40 Torr are the threshold of the self-limiting process, and that multilayer graphene starts to grow above this threshold. This breakdown in the self-limiting nature of the growth process is most likely due to a change in the rate limiting step of the process occurring at this pressure. Two fluxes can occur at simultaneously in the CVD process; mass-transport through the boundary layer and surface-reaction transport through the surface layer as shown in equations (1)–(3) where h_g is mass transport coefficient, K_s the surface reaction constant, C_g is the concentration of gas in the bulk, and C_s is the

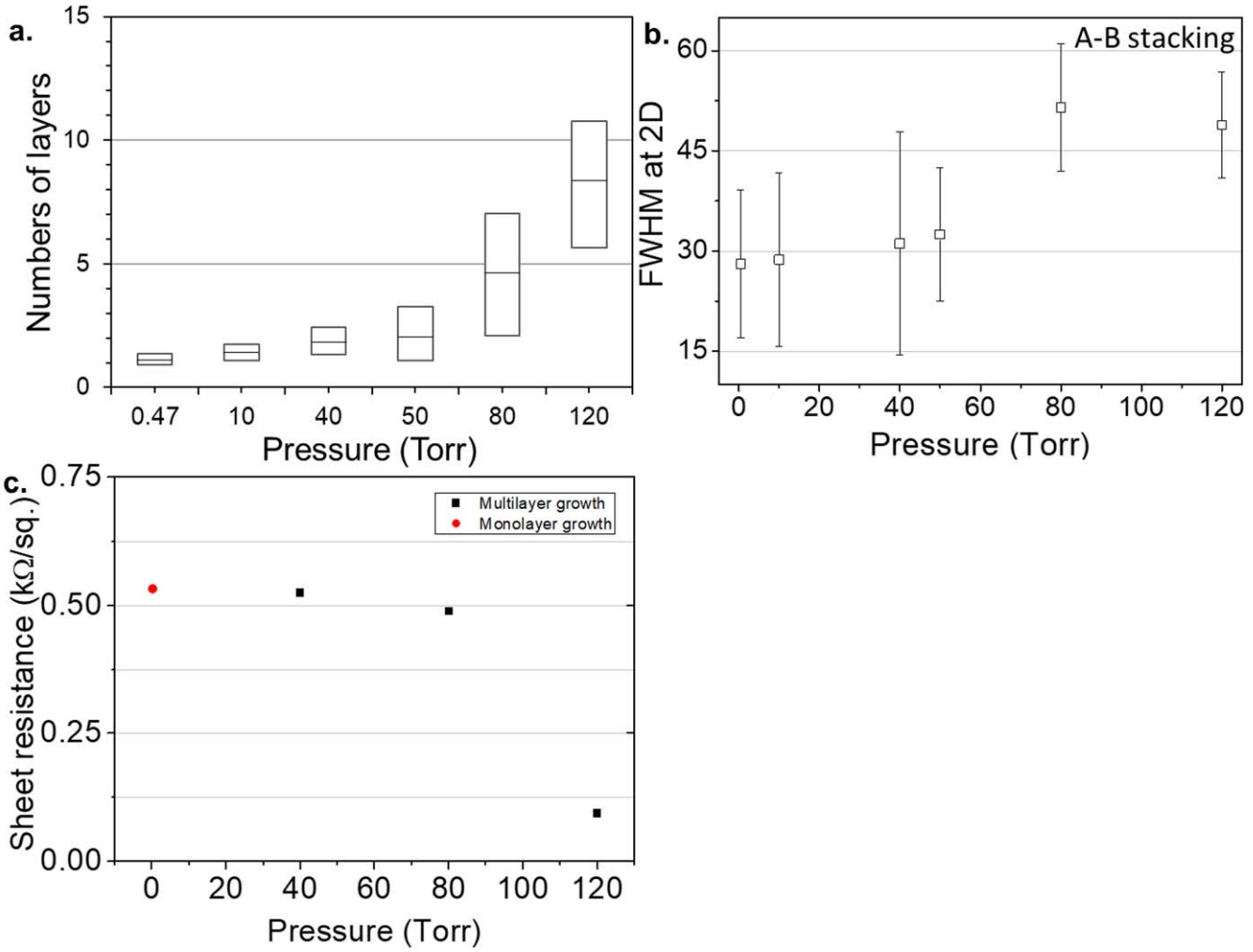

Figure 7. (a) Number of graphene layers as a function of the growth pressure in a box chart with average values of each growth condition marked as lines in the boxes. (b) Full-width at half maximum shown for each growth. (c) Measured sheet resistance of graphene transferred onto SiO_2/Si after growths from each growth pressure. Multilayer graphene exhibits reduced sheet resistance.

concentration of the active species at the surface [35]

$$F_{\text{mass-transport}} = h_g(C_g - C_s), \quad (1)$$

$$F_{\text{surface-transport}} = K_s C_s, \quad (2)$$

$$F_{\text{total-flux}} = C_g \frac{K_s h_g}{K_s + h_g}. \quad (3)$$

In CVD growth under low pressures, the surface transport reaction is the rate limiting step ($h_g \gg K_s$, $h_g \propto D_g$) since diffusivity through the boundary layer (D_g) formed on top of the catalyst substrate is inversely proportional to the growth pressure due to fewer collisions between molecules occurring within this boundary layer at lower pressures. Therefore, at low pressures, the graphene CVD growth process becomes limited by the surface transport mechanism, resulting in in the growth of monolayer graphene [35]. For growth processes closer to atmospheric pressure, mass transport through the boundary layer is the limiting rate step ($K_s \gg h_g$). Therefore, non-uniformities in the thickness of the boundary layer in the growth region can create changes in the uniformity of graphene layer and increase the number of active species that can diffuse into the surface and lead to the growth of additional graphene layers. The graphene growth conditions presented in this paper have a pressure range from mTorr to hundreds of Torr, which covers the low-pressure region where surface transport is the rate limiting step to the atmospheric region where mass-transport is the rate limiting step. The mass-transport and surface-transport growth mechanisms can co-exist in the transition (10–40 Torr). The mixture of these two growth regimes results in primarily bilayer graphene growth. Therefore, in this growth system, the pressure around 10–40 Torr defines the boundary between the two growth mechanisms well and where the self-limiting growth process that results in monolayer graphene growth at lower pressures starts to breakdown.

In order to determine how new multilayer structures are formed as the pressure increases and confirm the cause of the breakdown of the self-limiting growth process, the full-width at half maximum (FWHM) of the 2D peaks in each case was measured in order to determine the stacking order of graphene layers since it has been observed that AB stacking results in significant 2D peak broadening as compared with AA stacking [33]. Figure 7(b) shows FWHM of monolayer at

0.47 and 10 Torr was approximately 26 cm^{-1}, 27 cm^{-1}, respectively, suggesting that graphene synthesized on the copper foil is monolayer graphene. Large variations in the number of graphene layers occur when graphene is grown at pressures of 40 and 50 Torr. Depending on the location of the measurements, FWHM varied from 14 to 47 cm^{-1} with 40 Torr growths and 20 to 40 cm^{-1} with 50 Torr growths. Graphene growth this region is relatively sensitive to the growth pressure causing a large variation in the number of graphene layers that are formed. We believe that the threshold for breaking the self-limiting process occurs within this growth pressure range. The values of FWHM of the multilayer graphene was 50 cm^{-1} and 52 cm^{-1} at 80 Torr and 120 Torr, respectively, which indicates that the stacking order of the multilayer graphene is AB stacking. This is consistent with what would be expected under VW growth. Such results are reasonable since AB stacking is a more stable stacking order than the AA stacked graphene configuration [20]. (For further details of FWHM, please see figure S5 in supplementary information.) Therefore, as new layers are nucleated during the graphene growth process at higher pressures, stable AB stacking layers are formed with the graphene already present in the sample.

Finally, the sheet resistance as a function of the growth pressure was also measured as shown in figure 7(c). These results show that, as the growth pressure increases, there is a reduction in the sheet resistances of the samples, which is likely caused by the increased number of graphene layers in the samples [4]. This result confirms the results from the AFM/LFM and SEM measurements. However, the results also show that the change in sheet resistance is not a linear function of the average number of layers in the graphene. This is likely because the secondary layers of graphene grown below the primary graphene layer have not fully coalesced into a complete and uniform layer. Therefore, even though the sample might by >80% bilayer graphene, if the grains of the second graphene layer are not completely connected to each other, then the contact resistance between the grains on that layer might be so high that the second layer does not make a significant contribution to the overall electrical conductivity of the graphene structure [36]. This is supported by the fact that the electrical resistance does not start to drop until the pressure is >40 Torr which is when all of the measured spots on the graphene structure have at least two complete layers. Therefore, as the pressure increases above 40 Torr we would expect to see more complete layers forming and the sheet resistance to start to drop rapidly as is observed in figure 7(c).

Even though not all of the layers in the graphene might have fully coalesced, the electrical performance of the graphene produced using this growth method are still very good. The measured sheet resistance for the multilayer graphene is less than 100 Ω/sq. and the hole mobility of the graphene grown at 80 Torr, measured using a backgated FET with a drain voltage of 10 mV, is 412–643 $cm^2\,v^{-1}\,s^{-1}$. These results are consistent with the results for other graphene samples in the literature that are measured at room temperature and atmospheric pressure [4, 21, 37]. (See supplementary information figure S10 for more details.)

4. Conclusions

This paper shows that the number of graphene layers can be controlled by the pressure during growth. It demonstrates the successful growth of monolayer graphene at pressures below 10 Torr and up to 11 layers of graphene at pressures of 120 Torr. In addition, the multilayer graphene grows in an AB stacked sequence. A threshold of 10–40 Torr has also been identified for breaking the self-limiting process of graphene growth on Cu foil that typically results in only monolayer growth on graphene. There is also a threshold in the 40–80 Torr range where majority of the graphene grown changes from bilayer to multilayer. This threshold was also confirmed by the FWHM of the I_{2D} peak, where graphene grown at a pressure above 80 Torr has a FWHM of 50–60 cm^{-1}, whereas the FWHM is only 20–30 cm^{-1} at pressures below 50 Torr. Therefore, this work shows that by setting the pressure during the growth of graphene on copper substrates it is possible break the self-limiting growth mechanism and control the number of graphene layers that are grown.

Acknowledgments

This work is based upon work supported by the National Science Foundation under Cooperative Agreement No. EEC-1160494. We would like thank Dr Piner for AFM/LFM measurements and helpful discussions on multilayer graphene growth.

ORCID iDs

Joon Hyong Cho https://orcid.org/0000-0002-7329-2556

References

[1] Kim K S, Zhao Y, Jang H, Lee S Y, Kim J M, Kim K S, Ahn J-H, Kim P, Choi J-Y and Hong B H 2009 Large-scale pattern growth of graphene films for stretchable transparent electrodes *Nature* **457** 706
[2] Chen S *et al* 2011 Oxidation resistance of graphene-coated Cu and Cu/Ni alloy *ACS Nano* **5** 1321–7
[3] Zhang Y H *et al* 2014 The distribution of wrinkles and their effects on the oxidation resistance of chemical vapor deposition graphene *Carbon* **70** 81
[4] Bae S *et al* 2010 Roll-to-roll production of 30-inch graphene films for transparent electrodes *Nat. Nanotechnol.* **5** 574
[5] Gao L, Ni G-X, Liu Y, Liu B, Castro Neto A H and Loh K P 2013 Face-to-face transfer of wafer-scale graphene films *Nature* **505** 190
[6] Naghdi S, Rhee K Y and Park S J 2018 A catalytic, catalyst-free, and roll-to-roll production of graphene via chemical vapor deposition: low temperature growth *Carbon* **127** 1–12
[7] Ohta T, Bostwick A, Seyller T, Horn K and Rotenberg E 2006 Controlling the electronic structure of bilayer graphene *Science* **313** 951–4

[8] Das A *et al* 2008 Monitoring dopants by raman scattering in an electrochemically top-gated graphene transistor *Nat. Nanotechnol.* **3** 210
[9] Luo G, Zhang Z Z, Deng G W, Li H O, Cao G, Xiao M, Guo G C and Guo G P 2017 Coupling graphene nanomechanical motion to a single-electron transistor *Nanoscale* **9** 5608–14
[10] Bunch J S, van der Zande A M, Verbridge S S, Frank I W, Tanenbaum D M, Parpia J M, Craighead H G and McEuen P L 2007 Electromechanical resonators from graphene sheets *Science* **315** 490
[11] Oostinga J B, Heersche H B, Liu X, Morpurgo A F and Vandersypen L M K 2007 Gate-induced insulating state in bilayer graphene devices *Nat. Mater.* **7** 151
[12] Xia F, Farmer D B, Lin Y-m and Avouris P 2010 Graphene field-effect transistors with high On/Off current ratio and large transport band gap at room temperature *Nano Lett.* **10** 715–8
[13] Meric I, Han M Y, Young A F, Ozyilmaz B, Kim P and Shepard K L 2008 Current saturation in zero-bandgap, top-gated graphene field-effect transistors *Nat. Nanotechnol.* **3** 654
[14] Li X, Cai W, Colombo L and Ruoff R S 2009 Evolution of graphene growth on Ni and Cu by carbon isotope labeling *Nano Lett.* **9** 4268–72
[15] Lin H-C, Chen Y-Z, Wang Y-C and Chueh Y-L 2015 The essential role of Cu vapor for the self-limit graphene via the Cu catalytic CVD method *J. Phys. Chem.* C **119** 6835–42
[16] Pollard A J *et al* 2009 Formation of monolayer graphene by annealing sacrificial nickel thin films *J. Phys. Chem.* C **113** 16565–7
[17] Cho J H, Gorman J J, Na S R and Cullinan M 2017 Growth of monolayer graphene on nanoscale copper-nickel alloy thin films *Carbon* **15** 441–8
[18] Chen S, Cai W, Piner R D, Suk J W, Wu Y, Ren Y, Kang J and Ruoff R S 2011 Synthesis and characterization of large-area graphene and graphite films on commercial Cu–Ni alloy foils *Nano Lett.* **11** 3519–25
[19] Yao Y, Li Z, Lin Z, Moon K-S, Agar J and Wong C 2011 Controlled growth of multilayer, few-layer, and single-layer graphene on metal substrates *J. Phys. Chem.* C **115** 5232–8
[20] Ta H Q, Perello D J, Duong D L, Han G H, Gorantla S, Nguyen V L, Bachmatiuk A, Rotkin S V, Lee Y H and Rümmeli M H 2016 Stranski–Krastanov and Volmer–Weber cvd growth regimes to control the stacking order in bilayer graphene *Nano Lett.* **16** 6403–10
[21] Liu Q, Gong Y, Wilt J S, Sakidja R and Wu J 2015 Synchronous growth of AB-stacked bilayer graphene on Cu by simply controlling hydrogen pressure in CVD process *Carbon* **93** 199–206
[22] Luo Z, Lu Y, Singer D W, Berck M E, Somers L A, Goldsmith B R and Johnson A T C 2011 Effect of substrate roughness and feedstock concentration on growth of wafer-scale graphene at atmospheric pressure *Chem. Mater.* **23** 1441–7
[23] Sun H, Chen D, Wu Y, Yuan Q, Guo L, Dai D, Xu Y, Zhao P, Jiang N and Lin C-T 2017 High quality graphene films with a clean surface prepared by an UV/ozone assisted transfer process *J. Mater. Chem.* C **5** 1880–4
[24] Wang X, Dolocan A, Chou H, Tao L, Dick A, Akinwande D and Willson C G 2017 Direct observation of poly (methyl methacrylate) removal from a graphene surface *Chem. Mater.* **29** 2033–9
[25] Deng B *et al* 2017 Wrinkle-free single-crystal graphene wafer grown on strain-engineered substrates *ACS Nano* **11** 12337–45
[26] Na S R, Suk J W, Tao L, Akinwande D, Ruoff R S, Huang R and Liechti K M 2015 Selective mechanical transfer of graphene from seed copper foil using rate effects *ACS Nano* **9** 1325–35
[27] Li B W, Luo D, Zhu L, Zhang X, Jin S, Huang M, Ding F and Ruoff R S 2018 Orientation-dependent strain relaxation and chemical functionalization of graphene on a Cu(111) foil *Adv. Mater.* **30** 1706504
[28] Chae S J *et al* 2009 Synthesis of large-area graphene layers on poly-nickel substrate by chemical vapor deposition: wrinkle formation *Adv. Mater.* **21** 2328
[29] Han J, Lee J-Y and Yeo J-S 2016 Large-area layer-by-layer controlled and fully bernal stacked synthesis of graphene *Carbon* **105** 205–13
[30] Luo B, Chen B, Wang A, Geng D, Xu J, Wang H, Zhang Z, Peng L, Xu Z and Yu G 2016 Chemical vapor deposition of bilayer graphene with layer-resolved growth through dynamic pressure control *J. Mater. Chem.* C **4** 7464–71
[31] Wu R, Gan L, Ou X, Zhang Q and Luo Z 2016 Detaching graphene from copper substrate by oxidation-assisted water intercalation *Carbon* **98** 138–43
[32] Lee C, Wei X, Kysar J W and Hone J 2008 Measurement of the elastic properties and intrinsic strength of monolayer graphene *Science* **321** 385–8
[33] Huet B and Raskin J-P 2018 Role of Cu foil *in situ* annealing in controlling the size and thickness of CVD graphene domains *Carbon* **129** 270–80
[34] Nguyen V L *et al* 2015 Seamless stitching of graphene domains on polished copper (111) foil *Adv. Mater.* **27** 1376
[35] Bhaviripudi S, Jia X, Dresselhaus M S and Kong J 2010 Role of kinetic factors in chemical vapor deposition synthesis of uniform large area graphene using copper catalyst *Nano Lett.* **10** 4128–33
[36] Koepke J C, Wood J D, Estrada D, Ong Z-Y, He K T, Pop E and Lyding J W 2013 Atomic-scale evidence for potential barriers and strong carrier scattering at graphene grain boundaries: a scanning tunneling microscopy study *ACS Nano* **7** 75–86
[37] Reina A, Jia X, Ho J, Nezich D, Son H, Bulovic V, Dresselhaus M S and Kong J 2009 Large area, few-layer graphene films on arbitrary substrates by chemical vapor deposition *Nano Lett.* **9** 30–5